Inorg. Chem. **2006**, *45*, 3998–4006

Controllable Assembly of Metal-Directed Coordination Polymers under Diverse Conditions: A Case Study of the M^{II}–H_3tma/Bpt Mixed-Ligand System

Miao Du,* Xiu-Juan Jiang, and Xiao-Jun Zhao

College of Chemistry and Life Science, Tianjin Normal University, Tianjin 300074, P. R. China

Received January 1, 2006

A series of new metal–organic polymeric complexes, $\{[Co(bpt)(Htma)(H_2O)_3]\cdot 2.25H_2O\}_n$ (**1**), $[Co(bpt)(Htma)(H_2O)]_n$ (**2**), $[Ni(bpt)(Htma)(H_2O)]_n$ (**3**), $[Zn(bpt)_2(H_2tma)_2]\cdot 6H_2O$ (**4**), $\{[Cd(bpt)(Htma)(H_2O)]\cdot(C_2H_5OH)(H_2O)_{1.5}\}_n$ (**5**), and $\{[Cd(bpt)(Htma)(H_2O)_2]\cdot 5.5H_2O\}_n$ (**6**), was prepared from solution reactions of 4-amino-3,5-bis(4-pyridyl)-1,2,4-triazole (bpt) and trimesic acid (H_3tma) with different metal salts under diverse conditions. All these compounds were structurally determined by X-ray single-crystal diffraction, and the bulk new materials were further identified by X-ray powder diffraction. Complexes **1** and **6** show 1-D zigzag or linear Htma-bridged polymeric chains, with the terminal bpt ligands as pendants, which are extended to 2-D hydrogen-bonded arrays with 4.8^2 or (6,3) network topology. Coordination polymers **2** and **3**, in which the 2-D corrugated metal–organic frameworks make the interdigitated 3-D packing, are isostructural. Complex **4** has a mononuclear structure, and its subunits are hydrogen-bonded to each other to give a 2-D gridlike net. For complex **5**, the Cd^{II} centers are linked by bpt/Htma ligands to form a 2-D (4,4) coordination layer, and these layers are interdigitated in pairs. Notably, secondary noncovalent forces, such as hydrogen bonds, play an important role in extending and stabilizing these structural topologies. Interestingly, distinct products are obtained for Co^{II} (**1** and **2**) and Cd^{II} (**5** and **6**) under ambient or hydrothermal conditions; however, for Ni^{II} and Zn^{II}, single products, **3** and **4**, are generated. The thermal stabilities of **1**–**6** were studied by thermogravimetric analysis of mass loss. The desorption/adsorption properties of the porous material **5** are also discussed. Solid-state luminescent spectra of the Zn^{II} and Cd^{II} complexes, **4**–**6,** indicate intense fluorescent emissions at ca. 380 nm.

Introduction

The design and construction of polymeric metal−organic hybrid complexes are of considerable interest in recent years; the interest results from their appealing structural topologies and potential application in catalysis, adsorption/separation, host−guest chemistry, and the promising photo-, electro-, and magnetofunctional materials.[1−3] Generally, the diversity in the framework structures of such materials greatly depends on the selection of the metal centers and organic spacers, as well as on the reaction pathways.[1] Accordingly, ligands with certain functional groups, such as carboxylate, pyridyl, and phosphate, are especially crucial and have been widely explored.[4,5]

Several rational synthetic strategies have been proposed to achieve the metallosupramolecular arrays, and the most

* To whom correspondence should be addressed. Fax: 86-22-23540315. Tel: 86-22-23538221. E-mail: dumiao@public.tpt.tj.cn.

(1) (a) Braga, D.; Grepioni, F. *Coord. Chem. Rev.* **1999**, *183*, 19. (b) Leninger, S.; Olenyuk, B.; Stang, P. J. *Chem. Rev.* **2000**, *100*, 853. (c) Moulton, B.; Zaworotko, M. J. *Chem. Rev.* **2001**, *101*, 1629. (d) Zaworotko, M. J. *Chem. Commun.* **2001**, 1. (e) Carlucci, L.; Ciani, G.; Proserpio, D. M. *Coord. Chem. Rev.* **2003**, *246*, 247.

(2) Eddaoudi, M.; Moler, D. B.; Li, H.; Chen, B.; Reineke, T.; O'Keeffe, M.; Yaghi, O. M. *Acc. Chem. Res.* **2001**, *34*, 319. (b) Evans, O. R.; Lin, W. *Acc. Chem. Res.* **2002**, *35*, 511. (c) Tominaga, M.; Tashiro, S.; Aoyagi, M.; Fujita, M. *Chem. Commun.* **2002**, 2038. (d) Davis, M. E. *Nature* **2002**, *417*, 813. (e) Batten, S. R.; Murray, K. S. *Coord. Chem. Rev.* **2003**, *246*, 103. (f) Janiak, C. *Dalton Trans.* **2003**, 2781.

(3) Würthner, F.; Sautter, A. *Chem. Commun.* **2000**, 445. (b) Zimmerman, S. C.; Wendland, M. S.; Rakow, N. A.; Zharov, I.; Suslick, K. S. *Nature* **2002**, *418*, 399. (c) Rosi, N. L.; Eckert, J.; Eddaoudi, M.; Vodak, D. T.; Kim, J.; O'Keeffe, M.; Yaghi, O. M. *Science* **2003**, *300*, 1127. (d) Yaghi, O. M.; O'Keeffe, M.; Ockwing, N. W.; Chae, H. K.; Eddaoudi, M.; Kim, J. *Nature* **2003**, *423*, 705. (e) Tong, M.-L.; Kitagawa, S.; Chang, H, C.; Ohba, M. *Chem. Commun.* **2004**, 418.

(4) Wang, X. L.; Qin, C.; Wang, E. B.; Xu, L.; Su, Z. M.; Hu, C. W. *Angew. Chem., Int. Ed.* **2004**, *43*, 5036. (b) Mishra, A.; Wernsdorfer, W.; Abboud, K. A.; Christou, G. *J. Am. Chem. Soc.* **2004**, *126*, 15648. (c) Ye, B. H.; Tong, M. L.; Chen, X. M. *Coord. Chem. Rev.* **2005**, *249*, 545.

10.1021/ic060001d CCC: $33.50 © 2006 American Chemical Society
Published on Web 04/18/2006

effective one is to employ appropriate bridging building blocks capable of binding metal centers through direct dative bonds. As already known, the aromatic multicarboxyl ligands, such as phthalic, isophthalic, terephthalic, trimesic, and pyromellitic acid, are versatile modular components for realization of these extended systems.[6] Trimesic acid (H_3-tma), which possesses three symmetric exo-carboxyl groups around the benzene ring, has attracted considerable interest as a host for inclusion compounds with a wide variety of species[7] and also as an excellent organic spacer, which can exhibit diverse coordination fashions and bridge metal centers to assemble multidimensional architectures.[8] H_3tma can also behave as a trianion, dianion, or monoanion under different conditions and its degree of deprotonation would have great influence on the structures of the resulting coordination complexes.[8a]

On the other hand, rodlike *N*,*N*′-donor building blocks, such as the traditionally employed 4,4′-bipyridine, have been extensively studied in coordination chemistry,[9] and modification by introducing spacers between the two 4-pyridyl groups results in distinct spatial effects to produce unexpected architectures upon metal complexation.[10] We have focused intensively on the crystal engineering of an angular dipyridyl derivative, namely, 2,5-bis(4-pyridyl)-1,3,4-oxadiazole (bpo), from organic hydrogen-bonded solids to coordination polymers.[11] Recently, a related triazole-containing compound 4-amino-3,5-bis(4-pyridyl)-1,2,4-triazole (bpt) has attracted our attention as a continuation of this program.[12] Comparatively, bpt has a more bent backbone than bpo: the angle subtended at the center of the five-membered heterocyclic spacer and two pyridyl *N*-donors is 152° for bpt and 137° for bpo. Furthermore, the amino donor group can provide potential coordination or hydrogen bonding sites that will influence the final coordination architectures.

As far as the reaction pathways, a conventional synthetic method of solvent assembly has been carried out to obtain the target compounds. At one time, hydrothermal synthesis at mild temperature (100−200 °C) under autogeous pressure was proven to be a powerful approach in the preparation of low-soluble organic−inorganic hybrid materials, although the mechanism of the hydrothermal technique is still poorly understood.[13] As known, the resultant materials are also significantly dependent on a variety of factors, such as solvent medium, temperature, pH value, and molar ratio of reactants, and in some cases, two or more diverse species could be isolated under different synthetic conditions or strategies.[14] Thus, in this context, it is still a great challenge to obtain the predicted products at this stage.

Currently, the rational construction of new structurally defined metal−organic frameworks using the mixed-ligand strategy seems to be a marvelous success.[4c,12,13a,15] In our recent research, we have initiated a synthetic approach employing aromatic multicarboxylates and bpt upon reaction with different metal ions to construct new functional frameworks. A new type of 1-D + 2-D → 3-D polythreading topology with finite components and a 2-fold interpenetrating porous network assembled from Cu^{II} or Cd^{II} with mixed ligands bpt/terephthalate have been reported in the latest communication.[12] In this contribution, we will describe a series of M^{II}−H_3tma/bpt mixed-ligand metal−organic frameworks, which are interestingly regulated by metal ions and specific reactive conditions. The thermal stability, desorption/adsorption, and fluorescent emission of these new materials have also been discussed in detail.

Experimental Section

General Materials and Methods. With the exception of the ligand bpt, which was prepared according to the literature proce-

(5) Dalai, S.; Mukherjee, P. S.; Rogez, G.; Mallah, T.; Drew, M. G. B.; Chaudhuri, N. R. *Eur. J. Inorg. Chem.* **2002**, 3292. (b) Beitone, L.; Huguenard, C.; Gansmuller, A.; Henry, M.; Taulelle, F.; Loiseau, T.; Ferey, G. *J. Am. Chem. Soc.* **2003**, *125*, 9102. (c) Roesky, H. W.; Andruh, M. *Coord. Chem. Rev.* **2003**, *236*, 91. (d) Barnett, S. A.; Champness, N. R. *Coord. Chem. Rev.* **2003**, *246*, 145.

(6) Fun, H.-K.; Sundara Raj, S. S.; Xiong, R.-G.; Zuo, J.-L.; Yu, Z.; You, X.-Z. *J. Chem. Soc., Dalton Trans.* **1999**, 1915. (b) Vodak, D. T.; Braun, M. E.; Kim, J.; Eddaoudi, M.; Yaghi, O. M. *Chem. Commun.* **2001**, 2534. (c) Chen, X.-M.; Liu, G.-F. *Chem.—Eur. J.* **2002**, *8*, 4811. (d) Dybtsev, D. N.; Chun, H.; Kim, K. *Angew. Chem., Int. Ed.* **2004**, *43*, 5033. (e) Chu, D.-Q.; Xu, J.-Q.; Duan, L.-M.; Wang, T.-G.; Tang, A.-Q.; Ye, L. *Eur. J. Inorg. Chem.* **2001**, 1135. (f) Sun, D. F.; Cao, R.; Sun, Y. Q.; Bi, W. H.; Li, X. J.; Wang, Y. Q.; Shi, Q.; Li. X. *Inorg. Chem.* **2003**, *42*, 7512.

(7) Kolotuchin, S. V.; Fenlon, E. E.; Wilson, S. R.; Loweth, C. J.; Zimmerman, S. C. *Angew. Chem., Int. Ed. Engl.* **1995**, *34*, 2654. (b) Melendez, R. E.; Sharma, C. V. K.; Bauer, C.; Rogers, R. D.; Zaworotko, M. J. *Angew. Chem., Int. Ed. Engl.* **1996**, *35*, 2213.

(8) Yaghi, O. M.; Davis, C. E.; Li, G.; Li, H. *J. Am. Chem. Soc.* **1997**, *119*, 2861. (b) Dai, J.-C.; Wu, X.-T.; Fu, Z.-Y.; Cui, C.-P.; Hu, S.-M.; Du, W.-X.; Wu, L.-M.; Zhang, H.-H.; Sun, R.-Q. *Inorg. Chem.* **2002**, *41*, 1391. (c) Sun, D. F.; Cao, R.; Weng, J. B.; Hong, M. C.; Liang, Y. C. *J. Chem. Soc., Dalton Trans.* **2002**, 291. (d) Lin, Z. Z.; Jiang, F. L.; Chen, L.; Yuan, D. Q.; Hong, M. C. *Inorg. Chem.* **2005**, *44*, 73.

(9) Hagrman, P. J.; Hagrman, D.; Zubieta, J. *Angew. Chem., Int. Ed.* **1999**, *38*, 2639. (b) Blake, A. J.; Champness, N. R.; Hubberstey, P.; Li, W.-S.; Withersby, M. A.; Schröder, M. *Coord. Chem. Rev.* **1999**, *183*, 117. (c) Noro, S.; Kitaura, R.; Kondo, M.; Kitagawa, S.; Ishii, T.; Matsuzaka, H.; Yamashita, M. *J. Am. Chem. Soc.* **2002**, *124*, 2568.

(10) Hennigar, T. L.; MacQuarrie, D. C.; Losier, P.; Rogers, R. D.; Zaworotko, M. J. *Angew. Chem., Int. Ed. Engl.* **1997**, *36*, 972. (b) Carlucci, L.; Ciani, G.; Macchi, P.; Proserpio, D. M. *Chem. Commun.* **1998**, 1837. (c) Sharma, C. V. K.; Rogers, R. D. *Chem. Commun.* **1999**, 83. (d) Wang, Q. M.; Guo, G. C.; Mak, T. C. W. *Chem. Commun.* **1999**, 1849. (e) Brandys, M.-C.; Puddephatt, R. J. *Chem. Commun.* **2001**, 1508. (f) Pschirer, N. G.; Curtin, D. M.; Smith, M. D.; Bunz, U. H. F.; Zur Loye, H.-C. *Angew. Chem., Int. Ed.* **2002**, *41*, 583. (g) Carlucci, L.; Ciani, G.; Proserpio, D. M.; Rizzato, S. *CrystEngComm* **2003**, *5*, 190. (h) Wenger, O. S.; Henling, L. M.; Day, M. W.; Winkler, J. R.; Gray, H. B. *Inorg. Chem.* **2004**, *43*, 2043.

(11) Du, M.; Bu, X.-H.; Guo, Y.-M.; Liu, H.; Batten, S. R.; Ribas, J.; Mak, T. C. W. *Inorg. Chem.* **2002**, *41*, 4904. (b) Du, M.; Guo, Y.-M.; Chen, S.-T.; Bu, X.-H.; Batten, S. R.; Ribas, J.; Kitagawa, S. *Inorg. Chem.* **2004**, *43*, 1287. (c) Du, M.; Zhang, Z.-H.; Zhao, X.-J. *Cryst. Growth Des.* **2005**, *5*, 1199. (d) Du, M.; Zhang, Z.-H.; Zhao, X.-J. *Cryst. Growth Des.* **2005**, *5*, 1247.

(12) Du, M.; Jiang, X.-J.; Zhao, X.-J. *Chem. Commun.* **2005**, 5521.

(13) Tao, J.; Tong, M. L.; Shi, F. X.; Chen, X. M.; Ng, S. W. *Chem. Commun.* **2000**, 2043. (b) Feng, S.; Xu, R. *Acc. Chem. Res.* **2001**, *34*, 239. (c) Lu, J. Y. *Coord. Chem. Rev.* **2003**, *246*, 327.

(14) Jung, O.-S.; Park, S. H.; Kim, K. M.; Jang, H. G. *Inorg. Chem.* **1998**, *37*, 5781. (b) Withersby, M. A.; Blake, A. J.; Champness, N. R.; Cooke, P. A.; Hubberstey, P.; Li, W.-S.; Schröder, M. *Inorg. Chem.* **1999**, *38*, 2259. (c) Pan, L.; Huang, X. Y.; Li, J.; Wu, Y. G.; Zheng, N. W. *Angew. Chem., Int. Ed.* **2000**, *39*, 527. (d) Bu, X.-H.; Chen, W.; Hou, W.-F.; Du, M.; Zhang, R.-H.; Brisse, F. *Inorg. Chem.* **2002**, *41*, 3477. (e) Tong, M.-L.; Chen, X.-M.; Batten, S. R. *J. Am. Chem. Soc.* **2003**, *125*, 16170.

(15) Lu, J. Y.; Lawandy, M. A.; Li, J.; Yuen, T.; Lin, C. L. *Inorg. Chem.* **1999**, *38*, 2695. (b) Qi, Y. J.; Wang, Y. H.; Hu, C. W.; Cao, M. H.; Mao, L.; Wang, E. B. *Inorg. Chem.* **2003**, *42*, 8519. (c) Pedireddi, V. R.; Varughese, S. *Inorg. Chem.* **2004**, *43*, 450.

dure,[16] all reagents and solvents for the synthesis and analysis were commercially available and used as received. Fourier transform (FT) IR spectra (KBr pellets) were taken on an AVATAR-370 (Nicolet) spectrometer. Carbon, hydrogen, and nitrogen analyses were performed on a CE-440 (Leemanlabs) analyzer. Thermogravimetric analysis (TGA) experiments were carried out on a Dupont thermal analyzer from room temperature to 800 °C under N_2 atmosphere at a heating rate of 10 °C/min. X-ray powder diffraction (XRPD) data were recorded on a Rigaku D/max-2500 diffractometer at 60 kV and 300 mA for Cu Kα radiation ($\lambda = 1.5406$ Å), with a scan speed of 2 deg/min and a step size of 0.02° in 2θ. The calculated XRPD patterns were produced using the software PowderCell and single-crystal diffraction data. Fluorescence spectra of the polycrystalline powder samples were performed on a Cary Eclipse spectrofluorimeter (Varian) equipped with a xenon lamp and quartz carrier at room temperature.

Syntheses of the Complexes. {[Co(bpt)(Htma)(H_2O)$_3$]·2.25H_2O}$_n$ (1). An aqua solution (5 mL) of $Co(OAc)_2·4H_2O$ (25.0 mg, 0.10 mmol) was added to a hot EtOH (30 mL) solution of bpt (24.0 mg, 0.10 mmol) with stirring for 10 min. Then, a solution of H_3tma (22.0 mg, 0.10 mmol) in EtOH (5 mL) was added to the above mixture with continuous stirring for about 30 min. The resultant solution was filtered and left to stand at room temperature. Pink block crystals suitable for X-ray analysis were produced by slow evaporation of the solvent for 5 days in a 15% yield (9.0 mg, based on bpt). Anal. Calcd for $C_{21}H_{24.5}CoN_6O_{11.25}$: C, 42.36; H, 4.12; N, 14.01. Found: C, 42.44; H, 4.00; N, 14.21%. IR (KBr, cm^{-1}): 3338m, 3100w, 1699vs, 1631vs, 1540w, 1458w, 1252vs, 1214m, 1175vs, 1100vs, 926m, 836s, 772m, 747s, 684s, 625m.

[Co(bpt)(Htma)(H_2O)]$_n$ (2). A mixture of $Co(OAc)_2·4H_2O$ (30.0 mg, 0.12 mmol), bpt (24.0 mg, 0.10 mmol), H_3tma (21.0 mg, 0.10 mmol), and water (10 mL) was sealed in a Teflon-lined stainless steel vessel (20 mL), which was heated at 140 °C for 5 days and cooled to room temperature at a rate of 5 °C/h. Purple block crystals of **2** were collected in a 67% yield (35 mg, based on bpt). Anal. Calcd for $C_{21}H_{16}CoN_6O_7$: C, 48.20; H, 3.08; N, 16.06. Found: C, 47.83; H, 3.02; N, 15.96. IR (KBr, cm^{-1}): 3329m, 3083bs, 1690vs, 1611vs, 1548s, 1443s, 1365vs, 1280s, 1095w, 923w, 1720m, 1610vs, 1555s, 1362s, 1259s, 1097m, 1065w, 933m, 833s, 752s, 695s, 510s. 841m, 701m.

[Zn(bpt)$_2$(H_2tma)$_2$]·6H_2O (4) and {[Cd(bpt)(Htma)(H_2O)]·(C_2H_5OH)(H_2O)$_{1.5}$}$_n$ (5). The same synthetic procedure as that for **1** was used except that $Co(OAc)_2·4H_2O$ was replaced by $Zn(ClO_4)_2·6H_2O$ for **4** and $Cd(NO_3)_2·4H_2O$ for **5**, giving colorless block crystals, in 47% and 30% yields, respectively. Anal. Calcd for $C_{42}H_{42}ZnN_{12}O_{18}$ (**4**): C, 47.22; H, 3.96; N, 15.73. Found: C, 47.04; H, 3.94; N, 15.68. IR (KBr, cm^{-1}): 3637m, 3409s, 3336s, 3154m, 1700vs, 1626vs, 1585m, 1443m, 1386m, 1243s, 1173m, 1102m, 1063m, 1006m, 841m, 746s, 706m, 683m, 615m, 569m, 439m. Anal. Calcd for $C_{23}H_{25}CdN_6O_{9.5}$ (**5**): C, 42.51; H, 3.88; N, 12.94. Found: C, 42.10; H, 3.46; N, 12.88. IR (KBr, cm^{-1}): 3637m, 3409s, 3336s, 3154m, 1700vs, 1626vs, 1585m, 1443m, 1386m, 1243s, 1173m, 1102w, 1063w, 1006s, 841s, 746s, 706s, 683m, 615m, 569m, 507m.

[Ni(bpt)(Htma)(H_2O)]$_n$ (3) and {[Cd(bpt)(Htma)(H_2O)$_2$]·5.5H_2O}$_n$ (6). The same synthetic method as that for **2** was used except that $Co(OAc)_2·4H_2O$ was replaced by $Ni(OAc)_2·4H_2O$ for **3** and $Cd(NO_3)_2·4H_2O$ for **6**, yielding green block crystals for **3** and colorless needle crystals for **6**. Yield: 57% for **3**; 29% for **6**. Anal. Calcd for $C_{21}H_{16}NiN_6O_7$ (**3**): C, 48.22; H, 3.08; N, 16.07. Found: C, 48.02; H, 3.02; N, 16.14. IR (KBr, cm^{-1}): 3338m, 3083bs, 1689s, 1611s, 1542s, 1443s, 1368vs, 1281s, 1218m, 843m, 751m, 727m, 702m, 670m, 506w. Anal. Calcd for $C_{21}H_{29}CdN_6O_{13.5}$ (**6**): C, 36.30; H, 4.21; N, 12.11. Found: C, 36.97; H, 4.69; N, 12.01. IR (KBr, cm^{-1}): 3301s, 3173s, 1634w, 1602vs, 1554m, 1455s, 1403m, 1365m, 1332w, 1274w, 1222m, 1066w, 978m, 938s, 831vs, 733s, 701s, 607m, 511s.

Caution: Metal perchlorate complexes in the presence of organic ligand are potentially explosive. Only a small amount of material should be handled with care.

X-ray Crystallography. X-ray single-crystal diffraction data for **1**−**6** were collected on a Bruker Apex II CCD diffractometer at ambient temperature with Mo Kα radiation ($\lambda = 0.71073$ Å). There was no evidence of crystal decay during data collection. Semiempirical absorption corrections were applied (SADABS), and the program SAINT was used for integration of the diffraction profiles.[17a] All structures were solved by direct methods using the SHELXS program of the SHELXTL package and refined with SHELXL.[17b] The final refinements were performed by full-matrix least-squares methods with anisotropic thermal parameters for all non-hydrogen atoms on F^2. Generally, C-bound hydrogen atoms were placed geometrically and refined as riding atoms. For all the cases, the starting positions for hydroxyl hydrogen atoms were located in difference Fourier syntheses, and refinement proceeded using a rigid model, allowed to rotate but not tip. After they were located on the difference Fourier map, all amino H atoms were positioned geometrically and treated as riding atoms. With the exception of the solvate H atoms in **5** and **6** and all water hydrogens in **1**, which were not located, all other H atoms of the lattice and coordinated water in the structures of **2**−**6** were first located on difference Fourier maps, and then fixed at calculated positions and included in the final refinement. Isotropic displacement parameters of all H atoms were derived from the parent atoms. Further crystallographic details are summarized in Table 1.

Results and Discussion

Preparation and General Characterization of Complexes 1−6. Two different synthetic methods were applied in this work: solvent evaporation of the M^{II}−H_3tma/bpt mixture at room temperature and hydrothermal conditions. For Co^{II} and Cd^{II}, two different products (**1** and **2** for Co^{II}, **5** and **6** for Cd^{II}) were obtained via the two approaches, and for Ni^{II} and Zn^{II}, only species **3** and **4** were produced. Interestingly, if the purple crystals of **2** were kept in the mother liquid, after a period of ca. 1 week, a small amount of pink crystals of **1** were observed (identified by single-crystal X-ray diffraction). The compositions of all the new materials were determined by microanalytical and IR techniques. The phase purities of the bulk samples were identified by X-ray powder diffraction (XRPD, see Supporting Information, Figures S1−S6). Complexes **1**−**6** are air stable and can retain their structural integrity at room temperature for a considerable length of time. Notably, Zn^{II} complex **4** could also be isolated using the same preparation method; however, $Zn(OAc)_2$ was employed as the source of zinc (confirmed by X-ray diffraction, IR spectra, and elemental analyses).

(16) Bentiss, F.; Lagrenee, M.; Traisnel, M.; Mernari, B.; Elattari, H. *J. Heterocycl. Chem.* **1999**, *36*, 149.

(17) *SAINT*; Bruker AXS: Madison, WI, 1998. (b) Sheldrick, G. M. *SHELXTL NT*, version 5.1; University of Göttingen: Göttingen, Germany, 1997.

Table 1. Crystallography Data and Structure Refinement Summary for Complexes **1**−**6**

	1	**2**	**3**
chemical formula	$C_{21}H_{24.5}CoN_6O_{11.25}$	$C_{21}H_{16}CoN_6O_7$	$C_{21}H_{16}N_6NiO_7$
fw	599.9	523.33	523.11
cryst size (mm)	0.37 × 0.15 × 0.11	0.37 × 0.29 × 0.09	0.23 × 0.22 × 0.09
cryst syst	monoclinic	monoclinic	monoclinic
space group	$P2_1/n$	$P2_1/c$	$P2_1/c$
a (Å)	10.5223(12)	8.591(3)	8.5256(8)
b (Å)	19.109(2)	14.942(4)	15.0853(14)
c (Å)	13.7250(15)	16.870(5)	16.7476(16)
α (deg)	90	90	90
β (deg)	91.488(2)	94.883(4)	94.5770(10)
γ (deg)	90	90	90
V (Å^3)	2758.8(5)	2157.9(11)	2147.1(3)
Z	4	4	4
ρ_{calcd} (g/cm^3)	1.444	1.611	1.618
μ (mm^{-1})	0.689	0.854	0.963
F(000)	1238	1068	1072
total/independent reflns	14 711/4826	11 548/3802	11 524/3782
params	389	317	321
R_{int}	0.0362	0.0213	0.0249
R^a, $R_w{}^b$	0.0611, 0.1848	0.0289, 0.0882	0.0299, 0.0846
GOF^c	1.054	1.090	1.037
residuals (e Å^{-3})	0.867, −0.328	0.325, −0.234	0.326, −0.287

	4	**5**	**6**
chemical formula	$C_{42}H_{42}ZnN_{12}O_{18}$	$C_{23}H_{25}CdN_6O_{9.5}$	$C_{21}H_{29}CdN_6O_{13.5}$
fw	1068.25	649.89	693.90
cryst size (mm)	0.30 × 0.19 × 0.10	0.30 × 0.22 × 0.10	0.28 × 0.17 × 0.06
cryst syst	monoclinic	triclinic	triclinic
space group	$C2/c$	$P\bar{1}$	$P\bar{1}$
a (Å)	31.351(5)	10.2402(11)	10.1568(18)
b (Å)	8.4407(12)	11.0268(10)	12.287(2)
c (Å)	20.373(3)	13.0807(12)	13.938(2)
α (deg)	90	75.9540(10)	114.155(4)
β (deg)	122.321(2)	70.6970(10)	100.316(7)
γ (deg)	90	72.9590(10)	102.903(8)
V (Å^3)	4556.0(11)	1315.3(2)	1473.8(4)
Z	4	2	2
ρ_{calcd} (g/cm^3)	1.557	1.641	1.564
μ (cm^{-1})	0.631	0.895	0.814
F(000)	2208	658	706
total/independent reflns	12 774/4004	7224/4584	7828/5094
params	332	371	388
R_{int}	0.0267	0.0126	0.0299
R^a, $R_w{}^b$	0.0314, 0.0902	0.0234, 0.0632	0.0543, 0.1497
GOF^c	1.066	0.994	1.025
residuals (e Å^{-3})	0.289, −0.338	0.441, −0.339	0.846, −0.913

^{a} $R = \sum||F_o| - |F_c||/\sum|F_o|$. ^{b} $R_w = [\sum[w(F_o^2 - F_c^2)^2]/\sum w(F_o^2)^2]^{1/2}$. ^{c} GOF $= \{\sum[w(F_o^2 - F_c^2)^2]/(n - p)\}^{1/2}$.

This is also the case for **5** and **6**, suggesting that the final products are independent of the counteranions of the metal salts.

Structural Analysis of Complexes 1−6. Selected bond distances and angles for complexes **1**−**6** are listed in Table S1, and possible hydrogen-bonded parameters for these structures are presented in Table S2 (see Supporting Information).

{[Co(bpt)(Htma)(H$_2$O)$_3$]·2.25H$_2$O}$_n$ (1) and [Co(bpt)(Htma)(H$_2$O)]$_n$ (2). In complex **1**, each Co^{II} atom is six-coordinated and exhibits a distorted octahedral geometry. Three oxygens and a nitrogen atom from two Htma, one water donor, and a monodentate bpt ligand form the equatorial plane, and the other two water ligands occupy axial positions with an O7−Co1−O8 angle of 176.76(14)° (see Figure 1a). As depicted in Figure 1b, the Htma dianions act as bidentate bridging ligands, jointing the Co^{II} centers together to result in a 1-D polymeric [Co(Htma)]$_n$ chain along

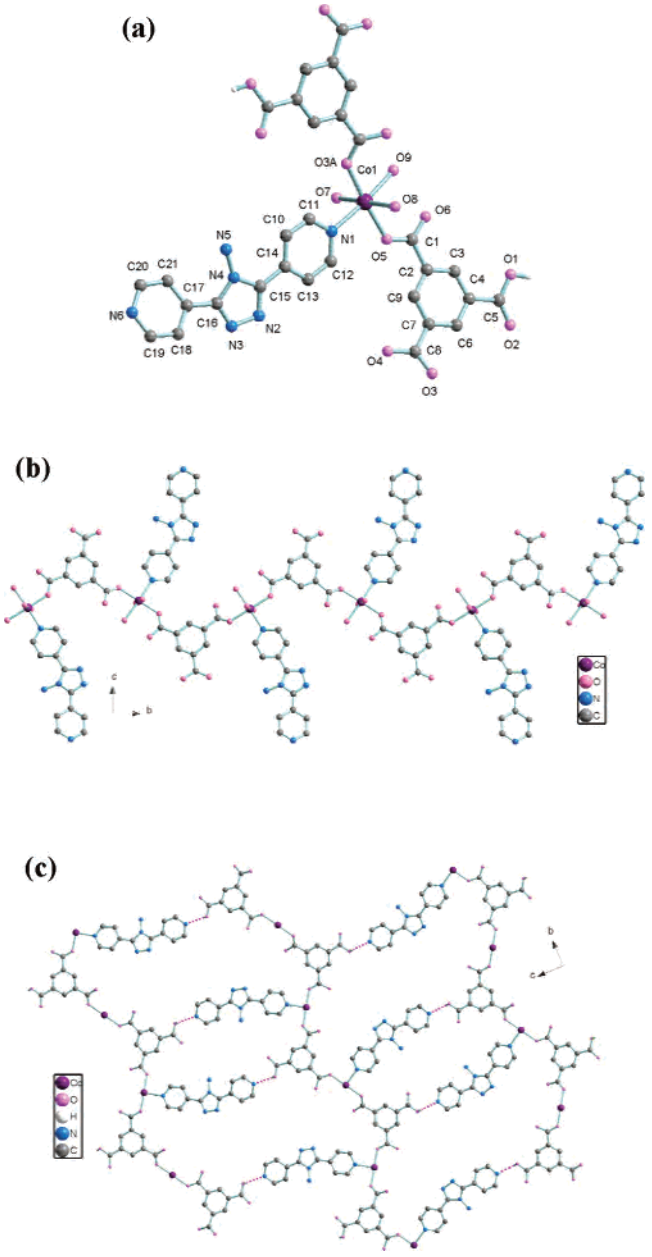

Figure 1. (a) Portion view of **1** with atom labeling of the asymmetric unit and metal coordination (lattice water molecules are omitted for clarity). (b) 1-D Htma-bridged chain with bpt decorated around each side. (c) A perspective view of the 2-D layered structure of **1** via interchain hydrogen bonds.

the crystallographic [010] direction. The crooked angle of the two carboxylates within each Htma makes the chain a wavelike arrangement, and the adjacent Co···Co separation is 9.723(1) Å. Notably, the terminal bpt ligands decorate the chain alternately in an outward fashion along two sides. These coordinated chains are extended into a 2-D sheet through interchain O−H···N hydrogen bonds between the carboxyl and "free" pyridyl nitrogen of bpt (see Figure 1c). Thus, if the strong hydrogen bonding is also considered, then both the Htma ligands and metal centers act as three-connecting nodes to produce an unusual 2-D 4.8^2 network.[18] Furthermore, such sheets are stacked in a parallel fashion

(18) Wells, A. F. *Three-Dimensional Nets and Polyhedra*; Wiley: New York, 1977.

with a little offset. As illustrated in Figure S7 (see Supporting Information), the centroid-to-centroid and face-to-face distances between the neighboring bpt and Htma segments are ca. 3.63 and 3.24/3.39 Å (with a dihedral angle of 5.8°), indicating the presence of significant interlayer $\pi-\pi$ stacking interactions.

In the 2-D metal−organic network of **2**, the coordination sphere of each central Co^{II} atom is provided by four oxygens and two nitrogens from two Htma, one water molecule, and two bpt ligands, displaying a distorted octahedral geometry (Figure 2a). The deviation of Co^{II} from the mean coordination plane, O5B−O6B−O1−N6A, is 0.004 Å, and the axial O7−Co1−N1 angle is 172.14(6)°. The Co^{II} centers are bridged by Htma (Co···Co distance = 8.756(2) Å), in which the carboxylates take the chelating bidentate and monodentate coordination modes, to produce wavelike 1-D polymeric chains, which are further extended by exo-bidentate bpt connectors (Co···Co distance = 14.226(10) Å) to produce a greatly corrugated 2-D (4,4) net (Figure 2b). Interestingly, investigation of the crystal packing shows that the Htma moieties, located up and down each 2-D array, insert into the lateral voids of the adjacent networks to produce an unusual interdigitated tactic motif (Figure 2c). In addition, the whole supramolecular lattice is further fixed via interlayer (O3−H3A···O4) and intralayer (O7−H7A···O2, O7−H7B···N3, N5−H5A···O5, and N5−H5B···O2) hydrogen bonds between the water, carboxylate, and amido groups (see Table S2 for details).

$[Ni(bpt)(Htma)(H_2O)]_n$ (3). Single-crystal X-ray diffraction analysis shows that complex **3** (Figure S8) is isomorphous to **2**. Two related 3-D porous frameworks $[Ni_6(tma)_4(bipy)_6(CH_3OH)_3(H_2O)_9\cdot(guest)]$ and $[Ni_3(tma)_2(bipy)_3(C_2H_6O_2)_3(H_2O)_3\cdot(guest)]$ (bipy = 4,4′-bipyridine) have been prepared by a layer-separation diffusion method.[19a] In both structures, the fully deprotonated tma trianions bridge the Ni^{II} centers to form rippled $[Ni_3(tma)_2]_n$ (6,3) layers, which are further extended by bipy pillars to generate 3-D architectures with large channels of 74% extraframework volume. This significant difference in structure of **3** may be attributed to the deprotonated levels of H_3tma. A more related example, namely, $[Ni_2(bipy)_3(Htma)_2(H_2O)](H_2O)$, was synthesized under conditions similar to those for **3**, and it also displays a 2-D coordinated net bridged by Htma and bipy; however, it is not as corrugated as **3**.[19b] This should result from the bent backbone of bpt. Of further interest, when naphthalene is introduced in the synthetic procedure, diversification of the hydrothermal products from 1-D chains, 2-D layers, and 3-D pillar-layered porous frameworks was found,[19b,19c] in which naphthalene plays key and different roles on the basis of the compositions of the starting reagents.

$[Zn(bpt)_2(H_2tma)_2]\cdot 6H_2O$ (4). Complex **4** has a windmill-like momonuclear structure that is disposed about a 2-fold axis. The central Zn^{II} atom is tetrahedrally coordinated (ZnO_2N_2) to two H_2tma and two bpt units, adopting the unidentate binding form and a trans arrangement (see Figure 4a). In each monodeprotonated H_2tma anion, one carboxyl group (O3−C17−O4) is hydrogen bonded (O3−H3···N1) to a "free" pyridyl nitrogen terminal. Thus, these monomeric molecules are linked to result in a 2-D (4,4) layered net with large rhombus grids (21.9 × 21.9 $Å^2$), as illustrated in Figure 4b. Interlayer N5−H5A···O5 hydrogen bonds are detected between the carboxyl and amido groups. The lattice water entities are located up and down the layers and form multiple

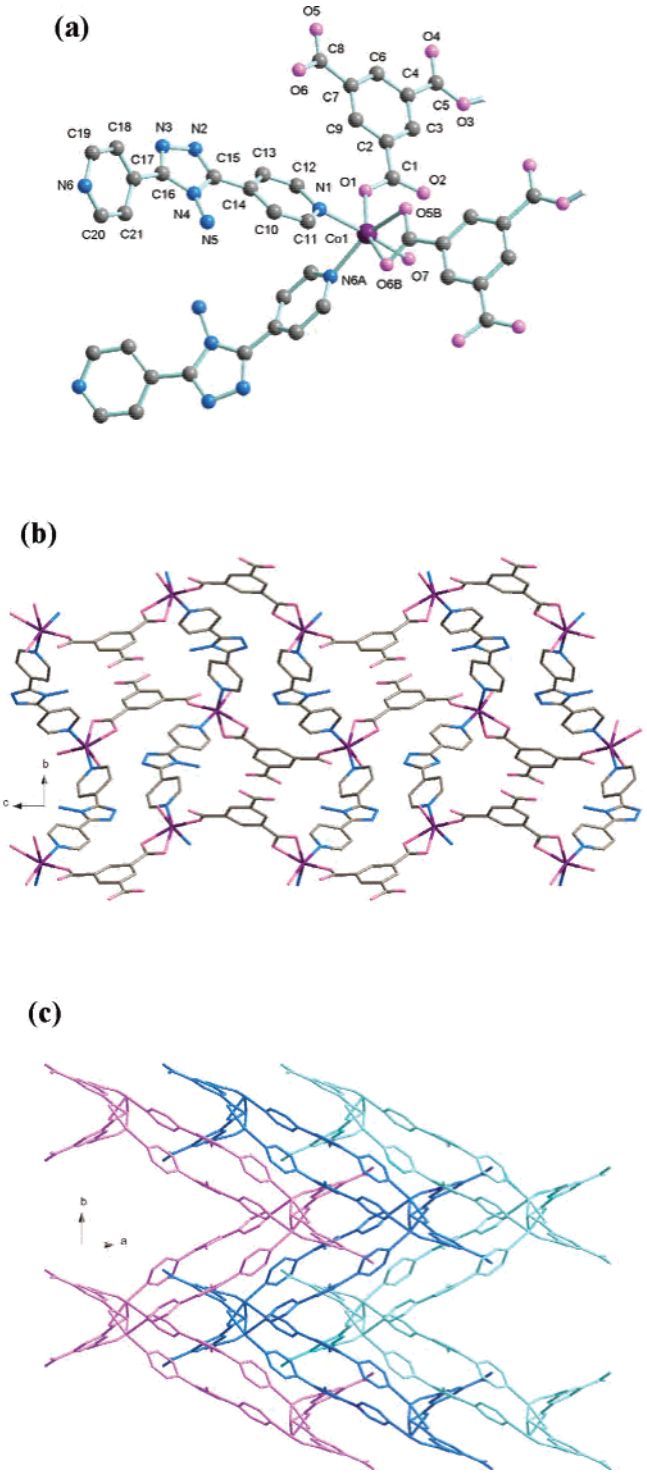

Figure 2. (a) View of **2** with atom labeling of the asymmetric unit and metal coordination. (b) 2-D corrugated coordination network of **2**. (c) A packing diagram of **2** showing the interdigitation of the 2-D nets.

(19) Prior, T. J.; Bradshaw, D.; Teat, S. J.; Rosseinsky, M. J. *Chem. Commun.* **2003**, 500. (b) Choi, E. Y.; Kwon, Y. U. *Inorg. Chem.* **2005**, *44*, 538. (c) Choi, E. Y.; Kwon, Y. U. *Inorg. Chem. Commun.* **2004**, *7*, 942.

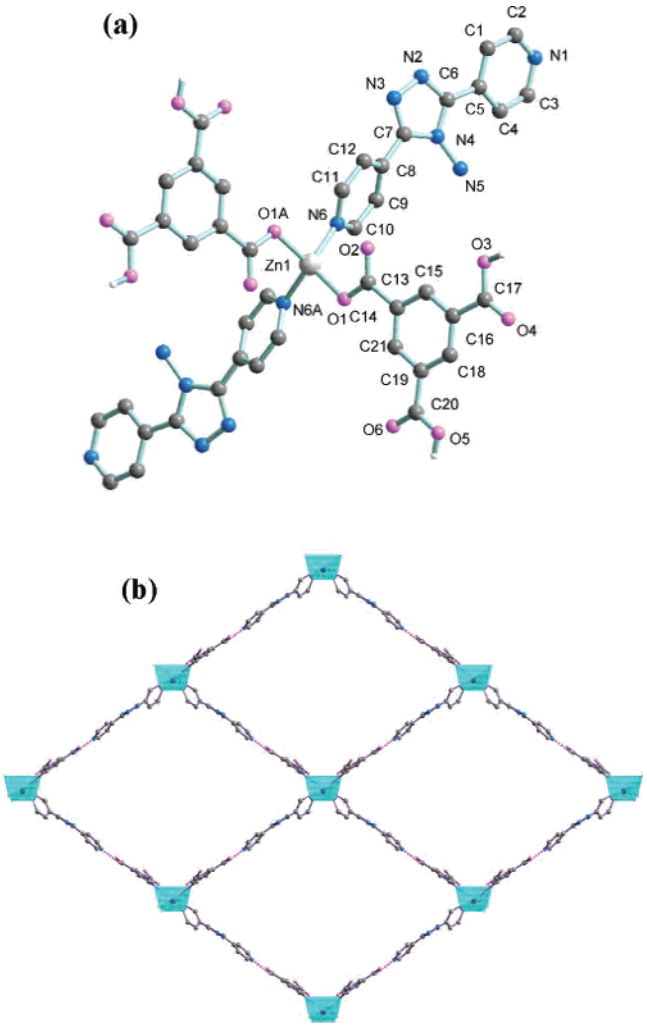

Figure 3. (a) Molecular structure of **4** with atom labeling of the asymmetric unit and metal coordination (lattice water moieties are omitted for clarity). (b) A perspective view of the 2-D hydrogen-bonded network of complex **4**.

water−water and water−layer hydrogen bonding interactions (see Table S2 for details), which further stabilize this structure.

{[Cd(bpt)(Htma)(H_2O)]·(C_2H_5OH)(H_2O)$_{1.5}$}$_n$ (5) and [Cd(bpt)(Htma)(H_2O)$_2$]·5.5H_2O}$_n$ (6). Complex **5** features a 3-D porous framework arising from 2-D coordination sheets interlinked through interlayer hydrogen bonds. The central Cd^{II} atom has a distorted octahedral coordination sphere defined by three oxygens from two separated Htma ligands, one aqua donor, and two nitrogens from a pair of bpt molecules (see Figure 4a). The O1, O2, O4A, and O7 atoms form the basal equatorial plane, and two nitrogen atoms take up the apical positions with a N6−Cd1−N1B angle of 164.44(10)°. Such fundamental building units are linked to furnish a 2-D layer with (4,4) topology via metal coordination, in which the Cd···Cd lengths bridged by Htma and bpt are 10.240(1) and 14.923(9) Å, respectively. In addition, a pair of adjacent 2-D patterns are antiparallel and interdigitated; the lateral Htma anions that orient on the same side of each layer penetrate into the 2-D grids, forming a supramolecular "double-layer" motif (see Figure 4b). Interlayer N5−H5B···O4 hydrogen bonds are detected to sustain

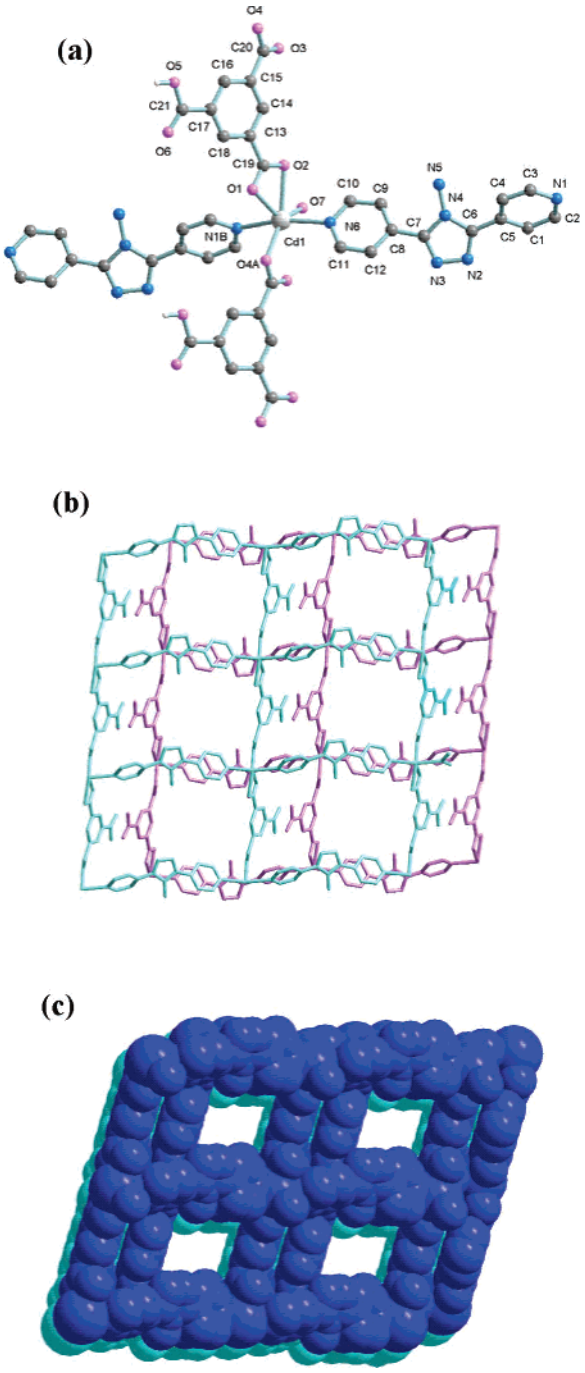

Figure 4. (a) View of **5** with atom labeling of the asymmetric unit and metal coordination (lattice solvates are omitted for clarity). (b) A view of a pair of opposite 2-D (4,4) coordination nets with interdigitated alignment. (c) Space filling model of the 3-D packing of **5** showing rectangular channels. The adjacent double-layer arrays are represented in different colors.

this array (see Figure S9). Interestingly, the water ligands of each double-layer motif are hydrogen bonded (O7−H7A···O6 and O7−H7B···O3) to the carboxyl groups of an adjacent such motif (Figure S9) to generate an extended 3-D framework (see Figure 4c). When viewed along the [010] direction, square channels are observed which are occupied by the disordered solvates. Computation of the channel space using PLATON[20] suggests a value of 279 Å^3, corresponding to 21.2% of the unit-cell volume. When an allowance is made

(20) Spek, A. L. *J. Appl. Crystallogr.* **2003**, *36*, 7.

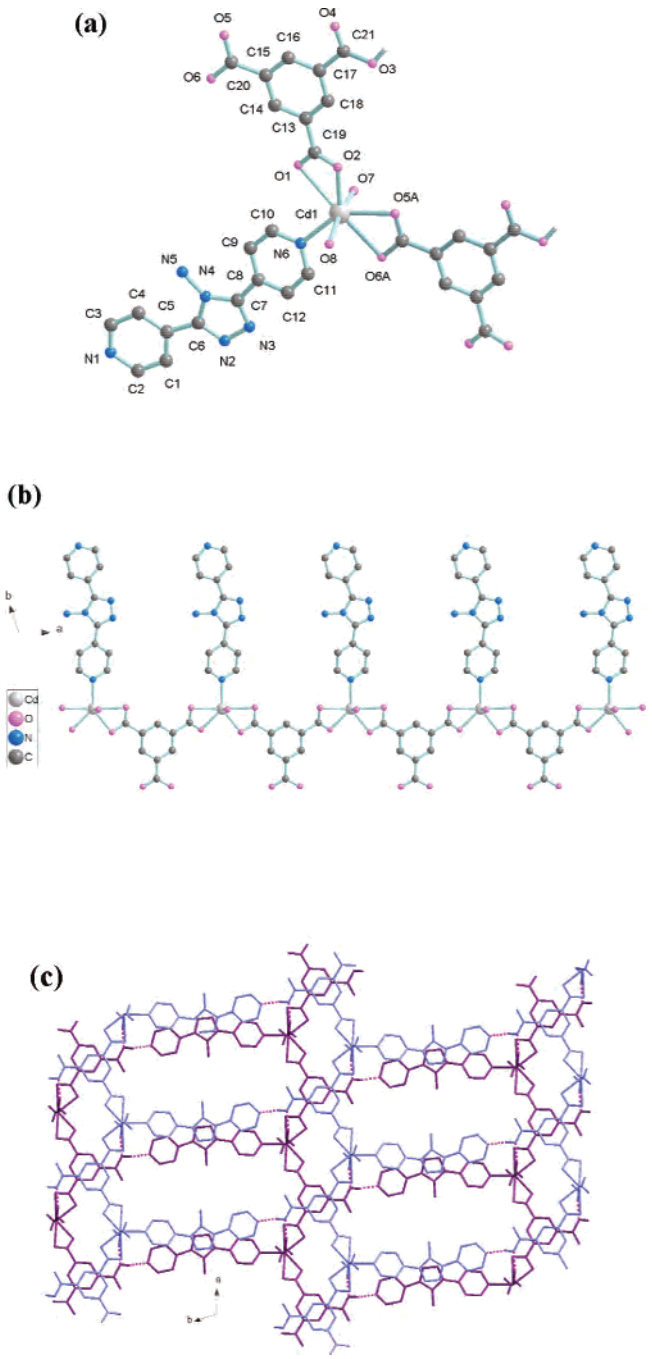

Figure 5. (a) View of **6** with atom labeling of the asymmetric unit and metal coordination (lattice water molecules are omitted for clarity). (b) 1-D Htma-bridged coordination chain with bpt decorated around one side. (c) A perspective view of the 2-D hydrogen-bonded double-layered network (the two layers are represented in different colors).

for the volume of the included solvate molecules, there is only 17 Å^3 of void space remaining. Additionally, there also are other O−H···O and N−H···O interactions in this structure (see Table S2 for details).

Complex **6** displays a polymeric chain coordination motif. As depicted in Figure 5a, the distorted pentagonal-dipyramidal coordination environment of the central Cd^{II} atom is provided by a pair of chelated carboxylate groups, one pyridyl nitrogen from bpt in the equatorial plane and two aqua moieties from apical sites. The Cd^{II} centers are propagated along the [100] direction via Htma bridges to form a 1-D linear array with bpt decorated on one side as terminal ligands (Figure 5b). The adjacent intrachain Cd···Cd distance is 10.157(2) Å. Similar to **1**, interchain O3−H3A···N1 hydrogen bonds between the carboxyl and pyridyl groups also link these 1-D chains to generate a 2-D hydrogen-bonded pattern, which, however, has a (6,3) network topology this time because of the discrepancy of two 1-D arrays in **1** and **6**. Moreover, the adjacent 2-D nets are combined into a double-layered architecture via interlayer O7−H7A···O3 interactions (see Figure 5c).

Obviously, the structural diversification of this series of mixed-ligand polymeric complexes should be attributed to the nature of the metal coordination as well as the synthetic approaches. The distinct structures of the Co^{II} and Cd^{II} complexes obtained under ambient or hydrothermal processes suggest that the synthetic condition can remarkably influence the formation of the final crystalline products. As a whole, from the viewpoint of coordination chemistry, Htma and bpt can behave as both bridging and terminal ligands in these complexes. For 2-D coordination polymers **2**, **3**, and **5**, the metal surroundings are taken up by two pairs of bpt/Htma and a water ligand, and the expansion of the 2-D nets along two directions is fulfilled via bpt/Htma connectors. For **1** and **6**, two Htma, one bpt, and water molecules occupy the metal coordination sites to reduce the valid linkage of the metal nodes in network generation. As a result, 1-D polymeric Htma-bridged chains are shaped with bpt only acting as terminal pendants. Additionally, the monodentate binding of H_2tma and bpt with Zn^{II} lead to the formation of mononuclear complex **4**. Investigation of these structures at a supramolecular level shows that different packing modes of **2** (or **3**) and **5** produce 3-D interdigitated or porous architectures. Interestingly, in the other three cases, hydrogen bonding between the carboxyl of Htma/H_2tma and the free pyridyl nitrogen of bpt link the 1-D or discrete coordination motifs to result in 2-D networks, however, with distinct 4.8^2, (4,4) or (6,3) topology, respectively. The synergistic effect of coordinative and second-sphere interactions will be responsible for the achievement of these well-regulated supramolecular structures.

Thermal Stability of the New Materials. Thermogravimetric experiments were conducted to study the thermal stability of **1**−**6**, which is an important parameter for metal−organic framework materials. The TGA curve of **1** suggests that the first weight loss of 7.02% in the region of 40−123 °C (peak at 114 °C) corresponds to the expulsion of the lattice water molecules (calculated 6.75%). The residual framework starts to decompose beyond 262 °C with a series of complicated weight losses (peaks at 328, 381, 463 and 704 °C) and does not stop until heating ends at 800 °C. The TGA curves of **2** and **3** are similar, probably because of their isostructural nature. The first weight loss of 3.78% in the 152−220 °C range for **2** (3.63%, 122−227 °C for **3**) is attributed to the removal of the coordinated water molecules (calculated 3.44%). The remaining substance is stable up to 310 °C for **2** (308 °C for **3**) followed by three consecutive steps of weight loss (peaks at 381, 449 and 708 °C for **2** and 408, 433 and 703 °C for **3**) and does not stop until

heating ends at 800 °C. For the TGA curve of **4**, the loss of lattice water moieties is not observed before 282 °C, where the decomposition starts, maybe because of the multiple strong hydrogen bonding interactions in the crystalline lattice. Further heating of the sample to 800 °C only reveals a continuous and slow weight loss. For the 3-D porous network **5**, a weight loss of 11.60% in the 46−165 °C (peak at 95 °C) corresponds to the release of the lattice water and ethanol guests (calculated 11.23%). Then the decomposition of the residual components starts beyond 195 °C with a series of complicated weight losses (peaks at 336, 382, 411 and 507 °C) and does not end until heating stops at 800 °C. For **6**, the weight loss of the lattice water (13.81%) occurs in the range of 45−260 °C (calculated 14.27%). The main framework remains intact until it is heated to 308 °C and then there are four steps of weight loss (peaks at 332, 386, 436 and 520 °C) that do not end until 800 °C.

Removal and Reintroduction of Guest Solvates. Metal−organic coordination polymers with specific channels or cavities have attracted considerable interest because of their potential applications in catalysis, adsorption, and ion exchange.[21] Complex **5** represents a fascinating 3-D supramolecular array exhibiting 1-D open cavities filled with solvates, as described above. The TGA results suggest that the ethanol and water guests could be excluded from the host framework upon heating. To further investigate the desorption/absorption properties of **5**, a freshly ground sample (97.6 mg) was placed inside a vacuum oven at 170 °C for 8 h. The sample experienced a weight loss of 11.2 mg, consistent with the removal of all included lattice solvates ($1.5H_2O + C_2H_5OH$) per formular unit (calculated, 11.0 mg). The XRPD pattern recorded at this point (see Figure 6) shows significant shifts of the sharp diffraction peaks compared with that of the original product. This indicates that the structure of the desolvated solid of **5** is changed; however, the high periodicity of this crystalline material still remains. Interestingly, the desolvated sample can regain the guest molecules and revert to the original structure by soaking in ethanol/water for 24 h. This is confirmed by XRPD (see Figure 6), the weight gain of the material (10.8 mg), and elemental analyses. Therefore, the framework integrity of **5** can be maintained after a desorption/adsorption cycle, and the desolvated solid of **5** may be useful as a potential adsorbent material for small guest molecules.

Photoluminescence Properties. The emission spectra of Zn^{II} and Cd^{II} (d^{10} metal) complexes **4**−**6**, together with those of the organic ligands bpt and H_3tma, in the solid state at room temperature are shown in Figure 7. The photoluminescence properties of bpt suggest a weak emission peak and an intense emission peak at 362 and 388 nm, respectively. The strongest emission peak for H_3tma appears at 365 nm, corresponding to the $\pi^* \rightarrow$ n transitions. For complexes **4**, **5**, and **6**, the maximum emission bands are at 380, 381 and 382 nm, respectively, which should come from intraligand $\pi \rightarrow \pi^*$ transitions. The blue-shift for such fluorescence peaks, compared to that of free bpt (388 nm), is the result of the incorporation of metal−ligand coordination interactions. Furthermore, considerable enhancement of the intensity for these peaks in the metal complexes may be attributed to the increased rigidity of the ligand when it is bound to a metal center, compared with that of the free one, which effectively reduces the loss of energy.[22] Additionally, the spectra of **4**−**6** also display a similar shoulder peak at ca. 360 nm, which probably results from the interplay of the intraligand transitions of two types of ligands. These results

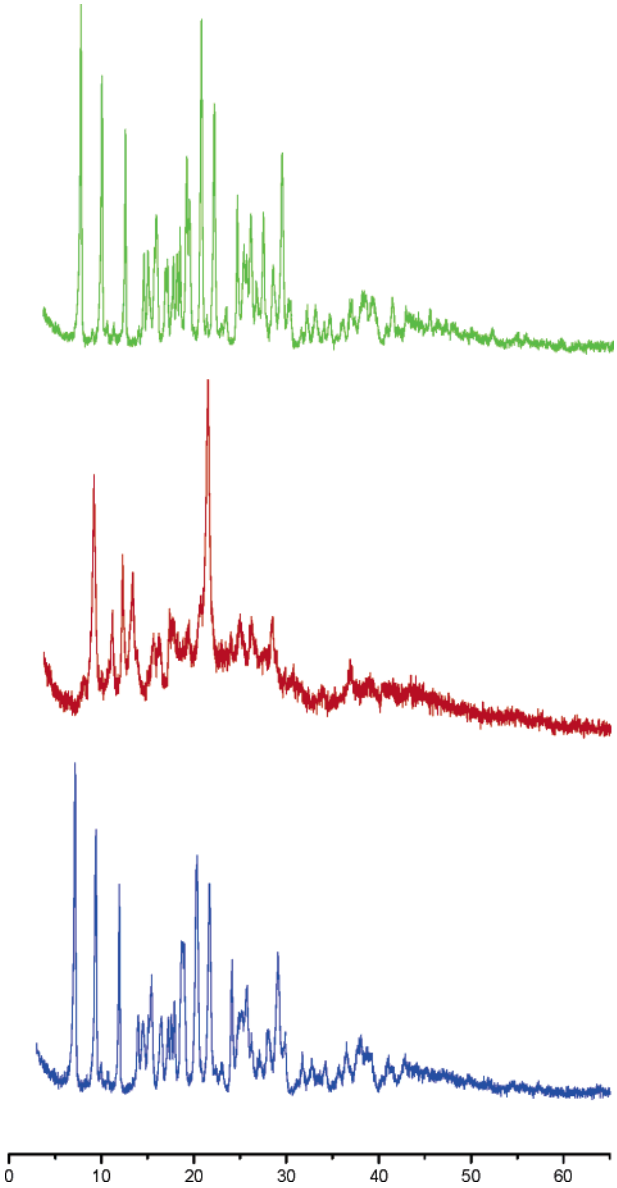

Figure 6. XPRD patterns for **5** recorded (green) at room temperature, (red) after removal of the guest solvates, and (blue) after reintroduction of the guest molecules.

(21) Sun, J.; Weng, L.; Zhou, Y.; Chen, J.; Chen, Z.; Liu, Z.; Zhao, D. *Angew. Chem., Int. Ed.* **2002**, *41*, 4471. (b) Pan, L.; Liu, H.-M.; Lei, X.-G.; Huang, X.-Y.; Olson, D. H.; Turro, N. J.; Li, J. *Angew. Chem., Int. Ed.* **2003**, *42*, 542. (c) Cui, Y.; Lee, S. J.; Lin, W. *J. Am. Chem. Soc.* **2003**, *125*, 6014. (d) Kitagawa, S.; Kitaura, R.; Noro, S. *Angew. Chem., Int. Ed.* **2004**, *43*, 2334. (e) Du, M.; Zhao, X.-J.; Guo, J.-H.; Batten, S. R. *Chem. Commun.* **2005**, 4836.

(22) Yi, L.; Zhu, L.-N.; Ding, B.; Cheng, P.; Liao, D.-Z.; Yan, S.-P.; Jiang, Z.-H. *Inorg. Chem. Commun.* **2003**, *6*, 1209. (b) Cai, L.-Z.; Chen, W.-T.; Wang, M.-S.; Guo, G.-C.; Huang, J.-S. *Inorg. Chem. Commun.* **2004**, *7*, 611.

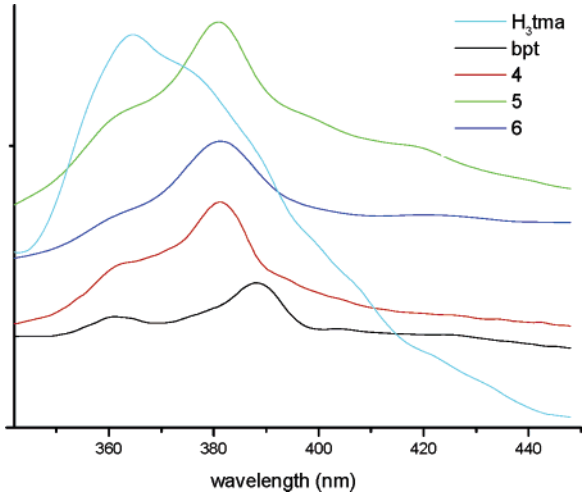

Figure 7. Solid-state fluorescence spectra recorded at room temperature for bpt, H_3tma, and complexes **4**−**6**.

indicate that such metal complexes could be good candidates for potential photoactive materials.

Conclusions and Perspectives

A new family of six metal-directed polymeric coordination complexes with mixed-ligand H_3tma and bpt has been prepared using diverse synthetic approaches, which exhibit interesting structural diversification. The mixed-ligand strategy seems to be a successful way to assemble programmed coordination frameworks. On one hand, H_3tma can be deprotonated at different levels, so it may behave as either a terminal or bridging connector (as well as bpt) to construct discrete or infinite coordination structures. On the other hand, the "free" carboxyl/pyridyl groups can also take part in the formation of specific hydrogen bonds to extend and sustain the final architectures. At this juncture, coordinative forces, as well as weak interactions, play a key role in structural assembly. Without doubt, this investigation tells us that the synthetic conditions can significantly influence the target products. However, at this stage, how to manipulate them in a certain direction is still a great challenge and more work is still need to extend this knowledge. In summary, this work is expected to provide new and important information for understanding and developing crystal engineering of metal−organic frameworks. From this perspective, further systematic studies for the design and synthesis, such coordination crystalline materials with bpt and other aromatic multicarboxylic acids, are under way in our lab.

Acknowledgment. This work was financially supported by the National Natural Science Foundation of China (20401012), the National Fundamental Research Project of China (2005CCA01200), the Key Project of Tianjin Natural Science Foundation (043804111), and the Key Project of Chinese Ministry of Education (205008).

Supporting Information Available: X-ray crystallographic files (CIF) for **1**−**6**, calculated and experimental X-ray powder diffraction (XRPD) patterns for **1**−**6**, three additional figures for complexes **1**, **3**, and **5**, and tables of bond parameters and hydrogen-bonded geometries for complexes **1**−**6**. This material is available free of charge via the Internet at http://pubs.acs.org.

IC060001D